Macromolecules

Article

Cite This: Macromolecules 2018, 51, 4415−4421

Morphology Transitions of Linear $A_1B_1A_2B_2$ Tetrablock Copolymers at Symmetric Overall Volume Fraction

Seonghyeon Ahn and Jin Kon Kim*

National Creative Research Initiative Center for Smart Block Copolymers, Department of Chemical Engineering, Pohang University of Science and Technology, Pohang, Kyungbuk 790-784, Republic of Korea

Bin Zhao, Chao Duan, and Weihua Li*

State Key Laboratory of Molecular Engineering of Polymers, Department of Macromolecular Science, Fudan University, Shanghai 200433, China

Supporting Information

ABSTRACT: We investigated morphology transitions of linear tetrablock copolymers of polystyrene-*block*-polyisoprene-*block*-polystyrene-*block*-polyisoprene ($S_1I_1S_2I_2$) by varying volume fraction of PI_1 block (f_{PI1}), while maintaining the symmetric volume fraction of total PS blocks and PI blocks ($f_{PS1}+f_{PS2}:f_{PI1}+f_{PI2} \approx 1:1$). An interesting sequence of morphology transitions was observed as f_{PI1} was increased: lamellae (L) → asymmetric lamellae (aL) → hexagonally packed PI-cylinders (C_{PI}) → double gyroid with PI-network domains (G_{PI}) → short-period lamellae (sL). The domain spacing of sL was nearly half that of L, while aL had asymmetric lamellar width of PS and PI microdomains. It is particularly interesting that cylindrical and gyroid morphologies were observed in linear block copolymers with symmetric overall volume fraction at intermediate segregation. The experimentally observed morphologies are in good agreement with the predicted equilibrium phases by self-consistent field theory (SCFT).

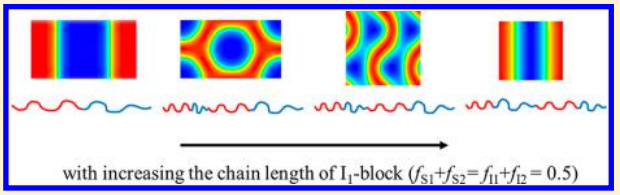

1. INTRODUCTION

Block copolymers have been extensively investigated because of their various nanostructures, depending on volume fraction, degree of polymerization (N), and the Flory−Huggins interaction parameter (χ).[1−4] For the phase diagram of a simple diblock copolymer, one of the controlling parameters is the volume fraction of one block. For example, hexagonally packed cylindrical microdomains have been found for AB diblock copolymers with volume fractions of one block (f_A) having 0.2−0.35, while lamellar microdomains were observed at f_A having 0.35−0.5.[1−4] However, binary blends of two block copolymers $(AB)_I$ and $(AB)_{II}$ where f_A in $(AB)_I$ is different from that in $(AB)_{II}$ showed unconventional microdomains not attained for neat AB diblock copolymer.[5−23] For example, Hashimoto and co-workers[9,10] showed that binary blends of two lamellar forming polystyrene-*block*-polyisoprene copolymers (PS-*b*-PI) with different molecular weights exhibited hexagonally packed cylinders, although the volume fraction of PS (f_{PS}) in one PS-*b*-PI was 0.53, while that in the other PS-*b*-PI was 0.55. Sakurai and co-workers[24,25] reported that binary blends of two cylinder-forming PS-*b*-PI with different f_{PS} (f_{PS} in one PS-*b*-PI was 0.65, while that of the other PS-*b*-PI was 0.26) showed gyroid microdomains when the overall volume fraction of PS block in the blend was 0.6. In addition, binary blends of AB and AC diblock copolymers where B and C blocks were capable of hydrogen bonding showed unconventional microdomains that could not be obtained by neat block copolymers of AB or AC.[21−23] We obtained highly asymmetric lamellar structure by blending asymmetric polystyrene-*block*-poly(2-vinylpyridine) copolymer (**as**-PS-*b*-2PVP) and asymmetric polystyrene-*block*-poly(4-hydroxystyrene) copolymer (**as**-PS-*b*-PHS), even though both neat **as**-PS-*b*-P2VP and **as**-PS-*b*-PHS were body-centered cubic (BCC) spherical microdomains, where the hydrogen bond was expected between P2VP and PHS.[21−23] Also, hexagonally packed cylindrical microdomains were obtained when a higher molecular weight of lamellar forming PS-*b*-P2VP was blended with a lower molecular weight of lamellar forming PS-*b*-PHS, where the volume fraction of total PS block in the blend was the same as that of P2VP + PHS blocks.[20]

Among many microstructures, cylindrical and gyroid structures have received great attention due to potential applications to nanoporous and advanced optical materials.[26−29] Wide ranges of the channel width in the gyroid structures would be needed to design a new optical material such as metamaterial because bandgap and effective plasma wavelength are easily adjusted by the channel size of gyroid structure.[30,31] However, gyroid structures are usually observed at a narrow range of volume fraction of A block (~0.35) in AB diblock copolymer. Also, to facilitate the flux in nanoporous

Received: March 16, 2018
Revised: May 3, 2018
Published: June 1, 2018

DOI: 10.1021/acs.macromol.8b00567
Macromolecules 2018, 51, 4415−4421

Table 1. Molecular Characteristics of $S_1I_1S_2I_2$ Employed in This Study

Sample	Mn[a] (kDa)	PDI[a]	f_{PS},total[b]	$f_{PS1,PI1,PS2,PI2}$[a,b]	τ_{PI}[c]	Schematic of Each Chain[d]	Morphology
SISI0	88.7	1.09	0.51	0.2/0/0.31/0.49	0		L
SISI17	71.8	1.15	0.54	0.22/0.08/0.32/0.38	0.17		aL
SISI24	82.1	1.07	0.51	0.18/0.12/0.33/0.37	0.24		C_{PI}
SISI30	97.8	1.07	0.54	0.23/0.14/0.31/0.32	0.30		C_{PI}
SISI34[e]	68.8		0.51	0.21/0.17/0.30/0.32	0.34		G_{PI}
SISI40	61.7	1.06	0.51	0.23/0.20/0.28/0.29	0.40		sL
SISI60	76.0	1.07	0.52	0.23/0.29/0.29/0.19	0.60		sL

[a]Determined by SEC based on PS standard. [b]Calculated by ^{1}H NMR with known density at room temperature (ρ_{PI}: 0.926; ρ_{PS}: 1.05). [c]$\tau_{PI} = (N_{PI1}/(N_{PI1} + N_{PI2})) = (f_{PI1}/(f_{PI1} + f_{PI2}))$. [d]Red and blue colors represent PS and PI, respectively. [e]SISSI34 was prepared by blending 35/65 (w/w) SISI24/SISI40. Mn, f_{PS},total, $f_{PS1,PI1,PS2,PI2}$, and τ_{PI} of the blend sample were calculated by average value of neat samples. L = lamellae, aL = asymmetric lamellae width of PS and PI microdomains, C_{PI} = hexagonally packed PI-cylinder, G_{PI} = double gyroid with PI-network domains, sL = short period lamellae.

materials with vertically aligned cylindrical pores, the pore volume should be increased. But, the pore volume obtained from cylindrical microdomains of AB diblock copolymer is at most ~0.35. Thus, one could not prepare pore volume larger than this value (say 0.5) because lamellar microdomains are expected instead of cylindrical microdomains at $f_A = 0.5$. Some research groups reported that miktoarm block copolymers (A_nB with $n \geq 2$) showed cylindrical and gyroid morphology at $f_A \sim 0.5$ depending on the number of arms.[32−34] Hadjichristidis and co-workers[33,34] reported that PI_2PS miktoarm block copolymer ($n = 2$) showed gyroid microdomains, while PI_3PS miktoarm block copolymer ($n = 3$) showed cylindrical microdomains at $f_{PS} \sim 0.5$. This suggests that the chain architecture can affect significantly phase behavior of block copolymers. In addition, Park et al.[35−37] reported that the disordered phase of nearly symmetric polystyrene-*block*-polymethylbutylene (PS-*b*-PMB) copolymer became cylindrical or gyroid microdomains depending on total molecular weights when sulfonate ion-conducting group was introduced to the PS chains.

Also, linear multiblock copolymers have shown unique microdomains that could not be obtained from AB diblock copolymers.[38−40] Sakurai and co-workers[38] reported morphology re-entry by changing the asymmetry of PS blocks ($\tau = f_{PS2}/(f_{PS1} + f_{PS2})$) in neat linear PS-*b*-polybutadiene-*b*-PS triblock copolymer at an overall volume fraction of PS blocks ($f_{PS1} + f_{PS2}$) having 0.64. With increasing τ the microdomains changed as gyroid → lamella → gyroid at $\chi N \sim 24$, while those changed as cylinder → lamealla → cylinder at $\chi N \sim 36$.

Very recently, Zhao et al.[41] predicted by using SCFT the phase behavior of linear $A_1B_1A_2B_2$ tetrablock copolymers depending on the asymmetry of A block ($\tau_A = N_{A1}/(N_{A1} + N_{A2})$) and B block ($\tau_B = N_{B1}/(N_{B1} + N_{B2})$), with N_i the degree of polymerization of the i block. For $0.2 < \tau_A < 0.6$, $\chi N = 60$ (in which N is the total polymerization degree in the tetrablock copolymer) and symmetric overall volume fractions of A and B block ($f_{A1} + f_{A2} = f_{B1} + f_{B2} = 0.5$), the microdomains changed from lamella to cylinder and gyroid and re-entry of lamella with increasing τ_B. Also, the domain spacing of lamellar microdomain at larger τ_B (>0.4) is about half of that at smaller τ_B (<0.15). Thus, even when the overall volume fraction of A blocks is the same as that of B blocks, cylinders (and even gyroids) could be formed.

In this study, we verified experimentally the re-entrant phase behavior of linear $A_1B_1A_2B_2$ tetrablock copolymers by changing the asymmetry of B blocks. For this, we synthesized, via anionic polymerization, $S_1I_1S_2I_2$ with various volume fractions (or chain lengths) of PI_1 and PI_2 blocks while keeping symmetric overall volume fraction of PS and PI blocks. We found, via small-angle X-ray scattering (SAXS) and transmission electron microscopy (TEM), that microdomains of $S_1I_1S_2I_2$ at a given $\tau_{PS} = 0.4$ were changed from lamellae with symmetric width (L), to lamellae with asymmetric width (aL), to hexagonally packed cylinders with PI chains (C_{PI}), then double gyroids with PI network domain (G_{PI}), and finally short-period lamellae with symmetric width (sL), with increasing the chain length of PI_1 block. The microdomain transitions are well consistent with those predicted by SCFT. C_{PI} and G_{PI} observed at a total volume fraction of PS blocks ~0.5 in linear $A_1B_1A_2B_2$ tetrablock copolymers are very interesting because cylinder microdomain is expected for the volume fraction of A block (f_A) having 0.2−0.35 (or 0.65−0.8) and gyroids for $f_A \sim 0.35$ (or 0.65) in AB diblock and ABA linear triblock copolymers.

2. EXPERIMENTAL SECTION

Materials. $S_1I_1S_2I_2$ tetrablock copolymers with various volume fractions of each block were synthesized by sequential anionic polymerization of styrene, isoprene, styrene, and isoprene in tetrahydrofuran (THF) at −78 °C under a purified argon atmosphere with benzyl potassium initiator. Styrene was polymerized for 1 h, and isoprene was polymerized for 4 h. At each step, we obtained aliquots by a syringe before addition of the next monomer.

Molecular Characterization. The number-average molecular weight (M_n) and polydispersity index (PDI) of various $S_1I_1S_2I_2$ samples as well as aliquots were measured by size exclusion chromatography (SEC: Waters 2414 refractive index detector) based on PS standards. Two 300 mm (length) × 7.5 mm (inner diameter) columns including particle size of 5 μm (PLgel 5 μm MIXED-C: Polymer Laboratories) were used with THF as an eluent and a flow rate of 1 mL/min at 30 °C. The volume fractions of each block were determined by SEC results of precursors and ^{1}H nuclear magnetic resonance spectra (^{1}H NMR: Bruker Avance III 400) with a solvent of chloroform-*d* ($CDCl_3$) (see Figures S1 and S2 in the Supporting Information). The molecular characteristics of samples are summarized in Table 1.

Sample Preparation. All samples were prepared by solution casting from 5 wt % THF solution and slowly evaporated at room

DOI: 10.1021/acs.macromol.8b00567
Macromolecules 2018, 51, 4415−4421

temperature (RT). For the complete removal of THF, samples were under vacuum for 24 h. Then, samples were thermally annealed at 240 °C for 2 h under high vacuum and quenched at RT. To fine-tune τ_{PI} between 0.24 and 0.40, we blended SISI24 and SISI40 (35/65 w/w) having τ_{PI} = 0.34.

Small-Angle X-ray Scattering (SAXS). SAXS profiles [$I(q)$ vs q (= $(4\pi/\lambda)$ sin θ), where q is the scattering vector and 2θ is the scattering angle] were obtained at the in-vacuum Undulator 20 beamline (4C SAXS II) of the Pohang Accelerator Laboratory (PAL) Korea. The wavelength and beam size were 0.675 Å and 0.2 (H) × 0.6 (W) mm^2, respectively. A two-dimensional charge coupled detector (Mar USA, Inc.) was used. The sample-to-detector distance was 4 m. The thickness of the sample was 1.0 mm, and the exposure time was 100 s.

Transmission Electron Microscopy (TEM). The samples were ultrasectioned using a Leica Ultracut Microtome (EM UC6 Leica Ltd.) at room temperature with a thickness of 40 nm. Then they were stained by exposure to OsO_4 vapor for 24 h at room temperature. The PI microdomains look dark in TEM images. The micrographs were taken at room temperature with bright-field TEM (S-7600 Hitachi Ltd.) at 80 kV.

3. RESULTS AND DISCUSSION

All samples showed unimodal and narrow molecular distribution (PDI < 1.15), as shown in SEC traces (Figure S1). Also, there was no peak corresponding to SIS triblock (or SI diblock and S homopolymer) due to using anionic polymerization. Thus, we successfully synthesized SISI0, SISI17, SISI24, SISI30, SISI40, and SISI60 with various τ_{PI} with a given τ_{PS} of 0.4 and the symmetric overall volume fraction of PS and PI blocks.

Figures 1 and 2 give SAXS profiles and TEM images of all samples. At τ_{PI} = 0, which is an SI diblock copolymer, the SAXS

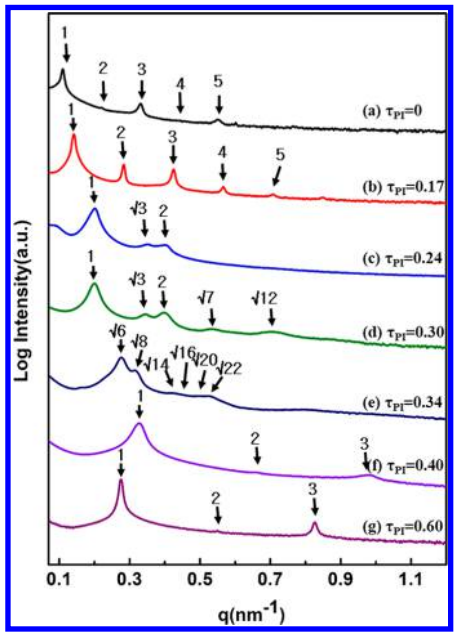

Figure 1. SAXS profiles of $S_1I_1S_2I_2$ samples: (a) SISI0, (b) SISI17, (c) SISI24, (d) SISI30, (e) SISI34, (f) SISI40, and (g) SISI60.

profile shows scattering peaks at positions of 1:2:3:4:5 relative to q^* (0.111 nm^{-1}). The lamellar domain spacing ($D = 2\pi/q^*$) obtained from SAXS profile was 57 nm. Very weak peaks at $2q^*$ and $4q^*$ indicate that SISI0 has symmetric lamellar width of PS and PI microdomains. This is consistent with the inset of TEM image in Figure 2a. At τ_{PI} = 0.17 of SISI17, although the SAXS profile also shows scattering peaks at positions of 1:2:3:4:5

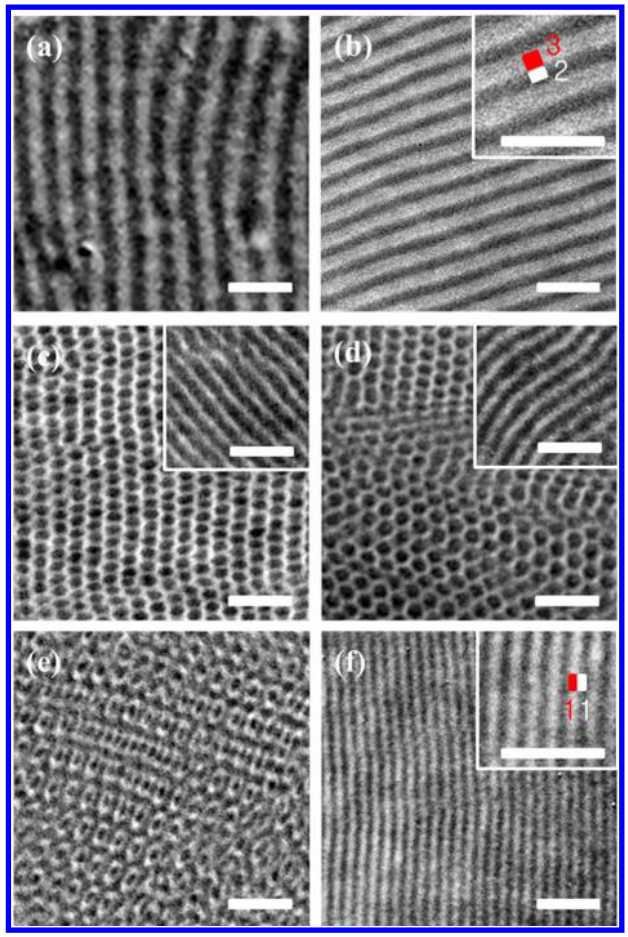

Figure 2. TEM images of $S_1I_1S_2I_2$ samples: (a) SISI0, (b) SISI17, (c) SISI24, (d) SISI30, (e) SISI34, and (f) SISI40. Dark regions correspond to PI microdomains due to selective staining of PI by OsO_4. Expanded TEM images in the insets of (b) and (f) show lamellar width ratios. The insets of (c) and (d) were obtained when samples were cut parallel to the cylinder axis. Scale bar of all images is 100 nm.

relative to q^* (0.142 nm^{-1} corresponding to D = 47 nm), it was different from that of SISI0. First, the domain spacing slightly decreased compared with that of SISI0. Second, the strong scattering peaks at $2q^*$ and $4q^*$ imply that the lamellar widths of PS and PI microdomains in SISI17 should be unequal. From the paracrystalline model fitting to SAXS profile (Figure S3), the predicted volume fraction of PS was 0.59. This is consistent with the observed lamellar width ratio of PS to PI microdomains (about 3:2) from TEM image (inset of Figure 2b). At τ_{PI} = 0.24−0.30, the scattering peaks at positions of $1:\sqrt{3}:2$ relative to q^* (0.200 nm^{-1} for SISI24; 0.199 nm^{-1} for SISI30) were observed. Thus, SISI24 and SISI30 showed hexagonally packed cylindrical morphologies. The domain spacing D (or the cylinder-to-cylinder distance d) was measured as 31 nm (or 36 nm) for the two samples. Well-ordered hexagonal packed cylinders were clearly seen in TEM images (Figure 2c,d) of SISI24 and SISI30. The volume fraction of the cylindrical cores from TEM image was estimated as almost 0.5. At $\tau_{PI} \sim 0.34$, the SAXS profile showed scattering peaks at positions of $\sqrt{6}:\sqrt{8}:\sqrt{14}:\sqrt{16}:\sqrt{18}:\sqrt{20}:\sqrt{22}$ relative to q^* (0.274 nm^{-1}), corresponding to double gyroid. Figure 2e shows the [110] projection of the double gyroid. The double gyroid morphology of SISI34 was further confirmed by birefringence

DOI: 10.1021/acs.macromol.8b00567
Macromolecules 2018, 51, 4415−4421

measurement because only SISI34 among all samples did not show any birefringence (Figure S4). When τ_{PI} was further increased, the scattering peaks became similar to those of SISI0, suggesting that the morphology was transformed back to symmetric lamellae. D of SISI40 and SISI60 was measured as 19 and 23 nm, respectively, which is nearly half of that of SISI0. In summary, by increasing τ_{PI}, the morphology of $S_1I_1S_2I_2$ transferred from symmetric lamellae (L) to asymmetric lamellae (aL) to hexagonally packed PI cylinders (C_{PI}) to double gyroid with PI network (G_{PI}) and finally to short-period symmetric lamellae (sL).

The transition sequence of morphologies of $S_1I_1S_2I_2$ as τ_{PI} is qualitatively consistent with the phase diagram predicted by SCFT in Figure 2 of ref 41. To make a more quantitative comparison, we identified the equilibrium morphologies of all experimental $S_1I_1S_2I_2$ samples using SCFT. Each polymer chain was coarse-grained into a freely jointed chain composed of Kuhn monomers with Kuhn length b. According to the standard definition of the free jointed chain model, the number of Kuhn monomers N for a specific polymer can be easily estimated. The Flory–Huggins parameter χ between PS and PI blocks was estimated as 0.043 at the annealing temperature (240 °C) according to the formula $\chi = 58/T - 0.07$.[42] A detailed calculation was found elsewhere.[41]

In Table 2, the free energies of possible morphologies for all $S_1I_1S_2I_2$ samples are listed. The equilibrium morphologies

Table 2. Free Energy per Chain of Various Ordered Mirodomains of $S_1I_1S_2I_2$ Samples Calculated by SCFT

	F/nk_BT[a]			
sample	L or aL	C_{PI}	G_{PI}	sL
SISI0	**6.119**			
SISI17	**8.536**	8.557	8.558	
SISI24	10.198	**10.022**	10.046	
SISI30		**11.184**	11.192	11.263
SISI34		11.398	**11.372**	11.374
SISI40		9.266	9.205	**9.137**
SISI60		10.428	10.284	**10.104**

[a]The free energy was calculated by the pseudospectral method of SCFT using the parameters provided in Table S1 of the Supporting Information. The free energy data of the equilibrium morphology of each sample are shown in bold font.

predicted by SCFT are L, aL, C_{PI}, C_{PI}, G_{PI}, sL, and sL for SISI0, SISI17, SISI24, SISI30, SISI34, SISI40, and SISI60, respectively, which are in good agreement with the experimental observations. Density color map and one-dimensional density distribution for each sample calculated by SCFT are given in Figure S5.

Figure 3 gives D-spacing change of $S_1I_1S_2I_2$ with τ_{PI} at a given $\tau_{PS} = 0.4$, normalized by D-spacing of SI diblock copolymer ($\tau_{PI} = 0$). Since the total molecular weight (M) of all $S_1I_1S_2I_2$ samples was not the same, we additionally normalized D by $N^{2/3}$ [43] because of different total molecular weight of the samples. Whether the relationship of D by $N^{2/3}$ holds for tetrablock copolymers, we obtained the dependence of D on N at fixed τ by the SCFT. As shown in Figure S6, D of the different morphologies formed in the tetrablock copolymers with various values of τ exhibits a very good scaling relationship as $D \sim N^{2/3}$.

The explanation of the change of D with τ_{PI} is as follows. As the symmetric lamellae transformed to asymmetric lamellae, the

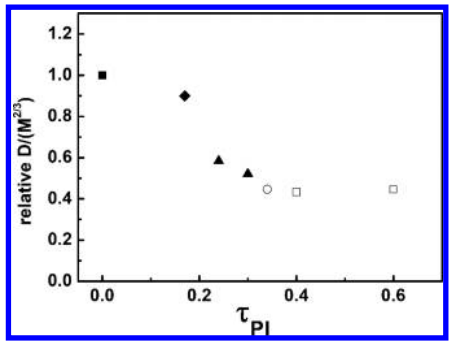

Figure 3. Change of D-spacing for $S_1I_1S_2I_2$ with τ_{PI} at a given $\tau_{PS} = 0.4$, normalized by D-spacing of SI diblock copolymer ($\tau_{PI} = 0$): (■) lamellae, (◆) asymmetric lamellae, (▲) cylinders, (○) gyroids, and (□) short-period lamellae.

D-spacing decreased slightly. This is because some PI_1 blocks form looping configuration, causing to decrease the D-spacing. However, the portion of looping PI_1 blocks is small, leading to a mild change in the D-spacing. When lamellar microdomains changed to C_{PI}, the D-spacing rapidly decreased. This is attributed to the fact that many PI_1 blocks migrate from the PS microdomain into the PI microdomain to overcome enthalpy penalty. In this situation, the portion of looping PI_1 blocks increased rapidly, resulting in a sudden drop of the D-spacing. Then, it gradually decreased when microdomains changed to G_{PI} and to lamellae because the remaining PI_1 blocks with bridge configuration are transformed to looping configuraiton. Interestingly, D at higher τ_{PI} is almost half of that of SI diblock copolymer, which is consistent with the prediction by SCFT.[41]

In ref 41, it has been argued that the morphology transitions are induced by the change of chain configurations in response to the change of block lengths. Importantly, a portion of the short PI_1 blocks is mixed into the PS microdomain via dangling configurations. At $\tau_{PI} = 0$, the copolymer becomes symmetric SI diblock, thus forming a lamellar morphology where each PS and PI microdomain consists of double-layer PS or PI chains (Figure 4a).

When τ_{PI} is slightly increased, most of the short PI_1 blocks prefer to being dangled in the PS microdomain instead of aggregating with the long PI_2 blocks. With τ_{PI} increasing, a decreased portion of PI_1 blocks swells the PS microdomain. Obviously, varying a portion of PI_1 blocks swelling PS microdomain leads to a change of the volume of PS microdomain or PI microdomain, i.e., the effective volume fraction of PS and PI microdomains ($f_{PS}^{eff} > 0.5$ or $f_{PI}^{eff} < 0.5$) differing from the total volume fraction of $S_1I_1S_2I_2$ tetrablock copolymer (e.g., $f_{PS} = f_{PI} = 0.5$). The swollen PS microdomain becomes larger than the PI microdomain, leading to asymmetric lamellae (aL) (Figure 4b). Then, the domain spacing is slightly decreased, consistent with the experimental result given in Figure 3. With SISI17 sample, $\tau_{PI} = 0.17$, the width ratio between PS and PI microdomains was measured about 3:2, i.e.$f_{PI}^{eff} \approx 0.4$ To Predict f_{PI}^{eff} depending on τ_{PI}, we performed SCFT calculation, and the result is given in Figure 4f. From Figure 4f, the predicted $f_{PI}^{eff} = 0.43$ at $\tau_{PI} = 0.17$, close to the TEM image (Figure 2b). To confirm the compatibility between PS block and PI_1 block in SISI17 sample, we performed differential scanning calorimetry (DSC) measurement. In SISI17, the glass transition temperature (T_g) of the PI block is the same as SISI0, but T_g of the PS block ($T_g = 96$ °C) is definitely lower than that (104 °C) of SISI0, even though

DOI: 10.1021/acs.macromol.8b00567
Macromolecules 2018, 51, 4415–4421

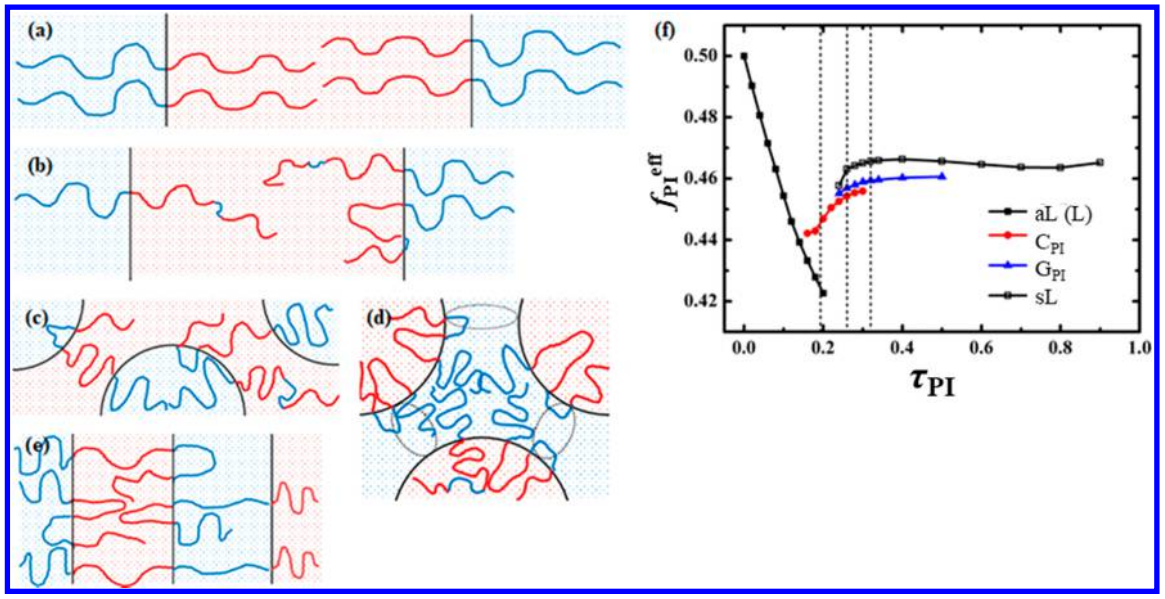

Figure 4. Schematics of major chain configurations in various microdomains (a–e). Blue and red denote PI and PS chains, respectively. (a) L, (b) aL, (c) C_{PI}, (d) G_{PI}, and (e) sL. (f) f_{PI}^{eff} of various ordered morphologies as a function of τ_{PI} for $xN = 60$ and $f_{PS1} = 0.2$. Three dashed lines indicate the transitions of aL → C_{PI} → G_{PI} → sL.

they have similar molecular weights (Figure S7). This indicates that some of PI chains are dissolved into the PS microdomain.

When τ_{PI} is further increased, the lamellar morphology transformed to the cylindrical morphology (Figure 4c). Surprisingly, an increase of f_{PI}^{eff} is accompanied by the transition to C_{PI} which is induced by the change of the chain configurations in response to the change of interfacial geometry. As the PI_1 block becomes long, the interfacial energy between PI_1/PS blocks becomes dominant over entropy, thus driving PI_1 blocks to migrate from the PS microdomain into the PI microdomain. The PI_1 blocks joining PI microdomains have to form loop configurations, causing an energy penalty. The energy penalty is relieved in curved interfacial geometries, thereby benefiting the formation of the C_{PI} morphologies compared with the lamellar morphology.

After passing the transition from aL to C_{PI}, increasing τ_{PI} increases f_{PI}^{eff} because longer PI_1 blocks are more separated from PS blocks and are mixed with PI_2 blocks. The increased f_{PI}^{eff} leads to G_{PI} morphology from C_{PI} morphology (Figure 4d). Because the entropy penalty for the formation of loop configuration of the PI_1 blocks in G_{PI} is smaller than that in LAM, G_{PI} becomes stable microdomains even at nearly symmetric effective volume fraction ($0.45 < f_I^{eff} < 0.46$).

When the PI_1 block is long enough ($\tau_{PI} > 0.34$), most PI_1 blocks are separated from PS blocks and are mixed with PI_2 blocks, leading to the formation of short-period lamellae because PI_1 and PS_2 blocks tend to form both loop and bridge configurations to maximize the configurational entropy (Figure 4e). Note from Figure 4f that f_{PI}^{eff} of the equilibrium morphologies varies nonmonotonically as τ_{PI} increases, i.e., decreasing to reach a minimum and then increasing to reach a near plateau. The changing effective volume fraction is the main factor resulting in the morphology transitions. The consistent results between experiment and theory confirm that the length of the inner chain has a significant effect on the morphology transitions of linear tetrablock copolymers.

4. CONCLUSION

A series of linear $S_1I_1S_2I_2$ tetrablock copolymers with symmetric volume fraction of PS/PI blocks were synthesized by sequential anionic polymerization, and their self-assembly behavior was studied by SAXS and TEM. With increasing the asymmetry of the PI_1 block, the morphology changed from lamellar to asymmetric lamellar, cylinder, double gyroid, and finally to short-period lamellar (half-domain size). The experimental results were consistent with the results of SCFT. The morphology mainly depended on the length of the PI_1 block. When the PI_1 block was short, some of the PI_1 blocks would stay inside the PS microdomain instead of joining the PI_2 blocks, which increased the effective volume fraction of the PS microdomain. Thus, the morphology changed from lamellae to asymmetric lamellae. When the PI_1 block was further increased, the interfacial energy between PI_1/PS blocks became dominant over entropy. In this situation, the PI_1 blocks joining PI microdomains have to form loop configurations, causing an energy penalty. This energy penalty was relieved in curved interfacial geometries, resulting in cylindrical microdomains and double gyroid. However, when the PI_1 block was long enough, PI_1 and PS_2 blocks tend to form both loop and bridge configurations to maximize the configurational entropy, causing re-entry of lamellae. An important conclusion from our study is that double gyroid and cylindrical microdomains could be formed in neat linear block copolymers with symmetric overall volume fraction.

■ ASSOCIATED CONTENT

Supporting Information

The Supporting Information is available free of charge on the ACS Publications website at DOI: 10.1021/acs.macromol.8b00567.

SEC chromatogram, ^{1}H NMR spectra, fitting data of SAXS profile with a variable lamellar thickness structure model, birefringence data, parameters of the experimental samples used in the calculations of SCFT, density color maps and one-dimensional density distribution

DOI: 10.1021/acs.macromol.8b00567
Macromolecules 2018, 51, 4415–4421

calculated by SCFT, domain spacing calculations of SCFT as a function of χN, DSC curves (PDF)

AUTHOR INFORMATION

Corresponding Authors

*E-mail jkkim@postech.ac.kr (J.K.K.).
*E-mail weihuali@fudan.edu.cn (W.L.).

ORCID

Jin Kon Kim: 0000-0002-3872-2004
Weihua Li: 0000-0002-5133-0267

Notes

The authors declare no competing financial interest.

ACKNOWLEDGMENTS

This work was supported by the National Creative Research Initiative Program, the National Research Foundation of Korea (2013R1A3A2042196), and the National Natural Science Foundation of China (Grants 21574026 and 21774025). SAXS experiments were conducted at 4C beamline of PAL (Korea).

REFERENCES

(1) Leibler, L. Theory of Microphase Separation in Block Copolymers. *Macromolecules* **1980**, *13* (6), 1602−1617.
(2) Bates, F. S.; Fredrickson, G. H. Block Copolymer Thermodynamics: Theory and Experiment. *Annu. Rev. Phys. Chem.* **1990**, *41* (1), 525−557.
(3) Kim, J. K.; Yang, S. Y.; Lee, Y.; Kim, Y. Functional Nanomaterials Based on Block Copolymer Self-Assembly. *Prog. Polym. Sci.* **2010**, *35* (11), 1325−1349.
(4) Kim, J. K.; Lee, J. I.; Lee, D. H. Self-Assembled Block Copolymers: Bulk to Thin Film. *Macromol. Res.* **2008**, *16* (4), 267−292.
(5) Court, F.; Hashimoto, T. Morphological Studies of Binary Mixtures of Block Copolymers. 1. Cosurfactant Effects and Composition Dependence of Morphology. *Macromolecules* **2001**, *34* (8), 2536−2545.
(6) Court, F.; Hashimoto, T. Morphological Studies of Binary Mixtures of Block Copolymers. 2. Chain Organization of Long and Short Blocks in Lamellar Microdomains and its Effect on Domain Size and Stability. *Macromolecules* **2002**, *35* (7), 2566−2575.
(7) Court, F.; Yamaguchi, D.; Hashimoto, T. Morphological Studies of Binary Mixtures of Block Copolymers: Temperature Dependence of Cosurfactant Effects. *Macromolecules* **2006**, *39* (7), 2596−2605.
(8) Court, F. o.; Yamaguchi, D.; Hashimoto, T. Morphological and Scattering Studies of Binary Mixtures of Block Copolymers: Cosurfactant Effects Observed in the Parameter Space of Temperature, Blend Composition, and Molecular Weight Ratio. *Macromolecules* **2008**, *41* (13), 4828−4837.
(9) Yamaguchi, D.; Hashimoto, T. A Phase Diagram for the Binary Blends of Nearly Symmetric Diblock Copolymers. 1. Parameter Space of Molecular Weight Ratio and Blend Composition. *Macromolecules* **2001**, *34* (18), 6495−6505.
(10) Yamaguchi, D.; Hasegawa, H.; Hashimoto, T. A Phase Diagram for the Binary Blends of Nearly Symmetric Diblock Copolymers. 2. Parameter Space of Temperature and Blend Composition. *Macromolecules* **2001**, *34* (18), 6506−6518.
(11) Kimishima, K.; Jinnai, H.; Hashimoto, T. Control of Self-Assembled Structures in Binary Mixtures of A− B Diblock Copolymer and A− C Diblock Copolymer by Changing the Interaction between B and C Block Chains. *Macromolecules* **1999**, *32* (8), 2585−2596.
(12) Vaidya, N. Y.; Han, C. D. Temperature-Composition Phase Diagrams for Binary Blends Consisting of Chemically Dissimilar Diblock Copolymers. *Macromolecules* **2000**, *33* (8), 3009−3018.
(13) Ahn, S.; Kwak, J.; Choi, C.; Seo, Y.; Kim, J. K.; Lee, B. Gyroid Structures at Highly Asymmetric Volume Fractions by Blending of ABC Triblock Terpolymer and AB Diblock Copolymer. *Macromolecules* **2017**, *50* (22), 9008−9014.
(14) Asai, Y.; Yamada, K.; Yamada, M.; Takano, A.; Matsushita, Y. Formation of Tetragonally-Packed Rectangular Cylinders from ABC Block Terpolymer Blends. *ACS Macro Lett.* **2014**, *3* (2), 166−169.
(15) Asai, Y.; Takano, A.; Matsushita, Y. Creation of Cylindrical Morphologies with Extremely Large Oblong Unit Lattices from ABC Block Terpolymer Blends. *Macromolecules* **2015**, *48* (5), 1538−1542.
(16) Asai, Y.; Takano, A.; Matsushita, Y. Asymmetric Double Tetragonal Domain Packing from ABC Triblock Terpolymer Blends with Chain Length Difference. *Macromolecules* **2016**, *49* (18), 6940−6946.
(17) Asari, T.; Matsuo, S.; Takano, A.; Matsushita, Y. Three-phase Hierarchical Structures from AB/CD Diblock Copolymer Blends with Complemental Hydrogen Bonding Interaction. *Macromolecules* **2005**, *38* (21), 8811−8815.
(18) Asari, T.; Arai, S.; Takano, A.; Matsushita, Y. Archimedean Tiling Structures from ABA/CD Block Copolymer Blends Having Intermolecular Association with Hydrogen Bonding. *Macromolecules* **2006**, *39* (6), 2232−2237.
(19) Chen, S.-C.; Kuo, S.-W.; Jeng, U.-S.; Su, C.-J.; Chang, F.-C. On Modulating the Phase Behavior of Block Copolymer/homopolymer Blends via Hydrogen Bonding. *Macromolecules* **2010**, *43* (2), 1083−1092.
(20) Han, S. H.; Kim, J. K.; Pryamitsyn, V.; Ganesan, V. Phase Behavior of Binary Blends of Block Copolymers Having Hydrogen Bonding. *Macromolecules* **2011**, *44* (12), 4970−4976.
(21) Han, S. H.; Pryamitsyn, V.; Bae, D.; Kwak, J.; Ganesan, V.; Kim, J. K. Highly Asymmetric Lamellar Nanopatterns via Block Copolymer Blends Capable of Hydrogen Bonding. *ACS Nano* **2012**, *6* (9), 7966−7972.
(22) Kwak, J.; Han, S. H.; Moon, H. C.; Kim, J. K.; Pryamitsyn, V.; Ganesan, V. Effect of the Degree of Hydrogen Bonding on Asymmetric Lamellar Microdomains in Binary Block Copolymer Blends. *Macromolecules* **2015**, *48* (17), 6347−6352.
(23) Kwak, J.; Han, S. H.; Moon, H. C.; Kim, J. K.; Koo, J.; Lee, J.-S.; Pryamitsyn, V.; Ganesan, V. Phase Behavior of Binary Blend Consisting of Asymmetric Polystyrene-*block*-poly (2-vinylpyridine) Copolymer and Asymmetric Deuterated Polystyrene-*block*-poly (4-hydroxystyrene). *Macromolecules* **2015**, *48* (4), 1262−1266.
(24) Sakurai, S.; Irie, H.; Umeda, H.; Nomura, S.; Lee, H. H.; Kim, J. K. Gyroid Structures and Morphological Control in Binary Blends of Polystyrene-*block*-polyisoprene Diblock Copolymers. *Macromolecules* **1998**, *31* (2), 336−343.
(25) Sakurai, S.; Umeda, H.; Furukawa, C.; Irie, H.; Nomura, S.; Hyun Lee, H.; Kon Kim, J. Thermally Induced Morphological Transition from Lamella to Gyroid in a Binary Blend of Diblock Copolymers. *J. Chem. Phys.* **1998**, *108* (10), 4333−4339.
(26) Park, S.; Wang, J.-Y.; Kim, B.; Xu, J.; Russell, T. P. A Simple Route to Highly Oriented and Ordered Nanoporous Block Copolymer Templates. *ACS Nano* **2008**, *2* (4), 766−772.
(27) Zalusky, A. S.; Olayo-Valles, R.; Wolf, J. H.; Hillmyer, M. A. Ordered Nanoporous Polymers from Polystyrene−Polylactide Block Copolymers. *J. Am. Chem. Soc.* **2002**, *124* (43), 12761−12773.
(28) Hsueh, H.-Y.; Yao, C.-T.; Ho, R.-M. Well-Ordered Nanohybrids and Nanoporous Materials from Gyroid Block Copolymer Templates. *Chem. Soc. Rev.* **2015**, *44* (7), 1974−2018.
(29) Hsueh, H.-Y.; Chen, H.-Y.; She, M.-S.; Chen, C.-K.; Ho, R.-M.; Gwo, S.; Hasegawa, H.; Thomas, E. L. Inorganic Gyroid with Exceptionally Low Refractive Index from Block Copolymer Templating. *Nano Lett.* **2010**, *10* (12), 4994−5000.
(30) Dolan, J. A.; Wilts, B. D.; Vignolini, S.; Baumberg, J. J.; Steiner, U.; Wilkinson, T. D. Optical Properties of Gyroid Structured Materials: From Photonic Crystals to Metamaterials. *Adv. Opt. Mater.* **2015**, *3* (1), 12−32.
(31) Vignolini, S.; Yufa, N. A.; Cunha, P. S.; Guldin, S.; Rushkin, I.; Stefik, M.; Hur, K.; Wiesner, U.; Baumberg, J. J.; Steiner, U. A 3D Optical Metamaterial Made by Self-Assembly. *Adv. Mater.* **2012**, *24* (10), OP23.

DOI: 10.1021/acs.macromol.8b00567
Macromolecules 2018, 51, 4415−4421

(32) Shi, W.; Lynd, N. A.; Montarnal, D.; Luo, Y.; Fredrickson, G. H.; Kramer, E. J.; Ntaras, C.; Avgeropoulos, A.; Hexemer, A. Toward Strong Thermoplastic Elastomers with Asymmetric Miktoarm Block Copolymer Architectures. *Macromolecules* **2014**, *47* (6), 2037−2043.
(33) Mavroudis, A.; Avgeropoulos, A.; Hadjichristidis, N.; Thomas, E. L.; Lohse, D. J. Synthesis and Morphological Behavior of Model 6-Miktoarm Star Copolymers, PS (P2MP) 5, of Styrene (S) and 2-methyl-1, 3-pentadiene (P2MP). *Chem. Mater.* **2006**, *18* (8), 2164−2168.
(34) Tselikas, Y.; Iatrou, H.; Hadjichristidis, N.; Liang, K.; Mohanty, K.; Lohse, D. Morphology of Miktoarm Star Block Copolymers of Styrene and Isoprene. *J. Chem. Phys.* **1996**, *105* (6), 2456−2462.
(35) Park, M. J.; Balsara, N. P. Phase Behavior of Symmetric Sulfonated Block Copolymers. *Macromolecules* **2008**, *41* (10), 3678−3687.
(36) Park, M. J.; Balsara, N. P.; Jackson, A. Order− Disorder Transitions in Block Copolymer Electrolytes at Equilibrium with Humid Air. *Macromolecules* **2009**, *42* (17), 6808−6815.
(37) Park, M. J.; Nedoma, A. J.; Geissler, P. L.; Balsara, N. P.; Jackson, A.; Cookson, D. Humidity-Induced Phase Transitions in Ion-Containing Block Copolymer Membranes. *Macromolecules* **2008**, *41* (6), 2271−2277.
(38) Sakurai, S.; Shirouchi, K.; Munakata, S.; Kurimura, H.; Suzuki, S.; Watanabe, J.; Oda, T.; Shimizu, N.; Tanida, K.; Yamamoto, K. Morphology Reentry with a Change in Degree of Chain Asymmetry in Neat Asymmetric Linear A1BA2 Triblock Copolymers. *Macromolecules* **2017**, *50* (21), 8647−8657.
(39) Adhikari, R.; Michler, G. H. Influence of Molecular Architecture on Morphology and Micromechanical Behavior of Styrene/butadiene Block Copolymer Systems. *Prog. Polym. Sci.* **2004**, *29* (9), 949−986.
(40) Masuda, J.; Takano, A.; Nagata, Y.; Noro, A.; Matsushita, Y. Nanophase-separated Synchronizing Structure with Parallel Double Periodicity from an Undecablock Terpolymer. *Phys. Rev. Lett.* **2006**, *97* (9), 098301.
(41) Zhao, B.; Jiang, W.; Chen, L.; Li, W.; Qiu, F.; Shi, A.-C. Emergence and Stability of a Hybrid Lamella−Sphere Structure from Linear ABAB Tetrablock Copolymers. *ACS Macro Lett.* **2018**, *7*, 95−99.
(42) Radlauer, M. R.; Sinturel, C.; Asai, Y.; Arora, A.; Bates, F. S.; Dorfman, K. D.; Hillmyer, M. A. Morphological Consequences of Frustration in ABC Triblock Polymers. *Macromolecules* **2017**, *50* (1), 446−458.
(43) Matsen, M.; Bates, F. S. Unifying Weak-and Strong-segregation Block Copolymer Theories. *Macromolecules* **1996**, *29* (4), 1091−1098.

DOI: 10.1021/acs.macromol.8b00567
Macromolecules 2018, 51, 4415−4421